Lee, Kim Fook; Tian, Ying; Yang, He; Mustonen, Kimmo; Martinez, Amos; Dai, Qing; Kauppinen, Esko I.; Malowicki, John; Kumar, Prem; Sun, Zhipei

Photon-Pair Generation with a 100 nm Thick Carbon Nanotube Film

Published in:
Advanced Materials

DOI:
10.1002/adma.201605978

Published: 27/06/2017

Document Version
Publisher's PDF, also known as Version of record

Please cite the original version:
Lee, K. F., Tian, Y., Yang, H., Mustonen, K., Martinez, A., Dai, Q., Kauppinen, E. I., Malowicki, J., Kumar, P., & Sun, Z. (2017). Photon-Pair Generation with a 100 nm Thick Carbon Nanotube Film. *Advanced Materials*, *29*(24), Article 1605978. https://doi.org/10.1002/adma.201605978

ADVANCED MATERIALS
www.advmat.de

Photon-Pair Generation with a 100 nm Thick Carbon Nanotube Film

Kim Fook Lee, Ying Tian, He Yang, Kimmo Mustonen, Amos Martinez, Qing Dai, Esko I. Kauppinen, John Malowicki, Prem Kumar, and Zhipei Sun**

Nonlinear optics based on bulk materials is the current technique of choice for quantum-state generation and information processing. Scaling of nonlinear optical quantum devices is of significant interest to enable quantum devices with high performance. However, it is challenging to scale the nonlinear optical devices down to the nanoscale dimension due to relatively small nonlinear optical response of traditional bulk materials. Here, correlated photon pairs are generated in the nanometer scale using a nonlinear optical device for the first time. The approach uses spontaneous four-wave mixing in a carbon nanotube film with extremely large Kerr-nonlinearity (≈100 000 times larger than that of the widely used silica), which is achieved through careful control of the tube diameter during the carbon nanotube growth. Photon pairs with a coincidence to accidental ratio of 18 at the telecom wavelength of 1.5 µm are generated at room temperature in a ≈100 nm thick carbon nanotube film device, i.e., 1000 times thinner than the smallest existing devices. These results are promising for future integrated nonlinear quantum devices (e.g., quantum emission and processing devices).

High purity photon-pair sources based on nonlinear optics are the essential ingredient for implementing unique properties of quantum mechanics such as entanglement and nonlocality, which are the foundation for various applications in quantum information processing.[1–3] Moving forward, it would be highly desirable to scale down these nonlinear optics-based quantum devices to the nanometer scale for compact and scalable operation of quantum information processing, but this direction remains largely unexplored experimentally.[1–3] Currently, the dominant nonlinear optical process used for the generation of high purity photon pairs at telecom wavelengths is based on spontaneous four-wave mixing (FWM) utilizing Kerr-nonlinearity.[4–10] Thus far, most FWM-based photon-pair sources utilize waveguide structures to enhance the Kerr nonlinearity of the used materials, such as highly nonlinear silica optical fibers[4,5] and silicon-on-insulator waveguides.[6,8] However, these approaches typically have large footprints and are not cost effective.[4–10] Fiber-based photon-pair sources, for example, typically require several tens of meters of silica fibers[4,5] (see Table S1 in Supporting Information for the current state of the art results with silica fibers and silicon waveguides). Nevertheless, scaling the length of these nonlinear optical devices down to the nanometer scale level is extremely challenging due to relatively small nonlinear optical response of traditional materials.

Single wall carbon nanotubes (SWNTs) recently have attracted intensive interest for electronic and optoelectronic applications (e.g., transistors, light sources, optical modulators, and photodetectors[11]) due to their electrical, optical,

---

Prof. K. F. Lee, Prof. P. Kumar
EECS Department
Northwestern University
Evanston, IL 60208, USA
E-mail: kim.lee@northwestern.edu

Prof. Y. Tian
Department of Physics
Dalian Maritime University
Dalian, Liaoning 116026, China

Prof. Y. Tian
Department of Applied Physics
Aalto University
FI -00076 Aalto, Finland

H. Yang, Prof. Z. Sun
Department of Electronics and Nanoengineering
Aalto University
FI -00076 Aalto, Finland
E-mail: zhipei.sun@aalto.fi

Dr. K. Mustonen, Prof. E. I. Kauppinen
Department of Applied Physics
Aalto University
FI 00076, Aalto, Finland

Dr. A. Martinez
Aston Institute of Photonic Technologies
Aston University
Aston Triangle, Birmingham B4 7ET, UK

Prof. Q. Dai
National Center for Nanoscience and Technology
Beijing 100190, China

J. Malowicki
Air Force Research Laboratory
Rome, NY 13441, USA

DOI: 10.1002/adma.201605978

and mechanical properties.[11] SWNTs also have been utilized for various nonlinear all-optical devices (for example, ultrafast pulsed lasers,[12] optical limiters,[13] and wavelength converters[14–16]) in the classical domain. Further, SWNTs can be easily and cost-effectively fabricated and integrated with other material-based devices/systems (e.g., optical fibers[12] and silicon waveguides[17]) for hybrid electronic and optoelectronic device integration. Recently, it has been shown that linear-optical quantum devices using carbon nanotubes[18–21] and two-dimensional (2D) layered materials[22–25] exhibit single-photon quantum correlation. However, these concepts are not compatible with existing dominant integrated photonic networks at 1.5 μm due to the mismatch between the generated quantum-states and existing fiber/silicon waveguide devices in spatial, spectral, and polarization domains.

In this work, for the first time, we demonstrate quantum-state generation in a nanometer scale nonlinear optic device consisting of a ≈100 nm thick carbon nanotube film. To do this, we maximize the third order nonlinearity of the nanotube device by carefully controlling the tube diameter during the carbon nanotube growth. We investigate the classical and quantum noise of photons generated in SWNTs by characterizing the quantum correlation of generated photon-pairs through the measurement of coincidence to accidental ratio (CAR, analogous to the signal-to-noise ratio). We obtain a maximum CAR of 18 with a production rate of 3.3×10^{-4} per pulse (corresponding to ≈16 667 photon pairs per second). The CAR is limited by Raman scattering processes, which can be suppressed by cooling the SWNT device.

Our SWNTs were synthesized using a spark discharge-based floating catalyst chemical vapor decomposition (FC-CVD) method with iron (Fe) particles as catalysts and carbon monoxide (CO) as carbon precursor (**Figure 1**a,b, details as described in the Experimental Section).[26] Figure 1c shows a scanning electron microscope (SEM) image of the SWNT device. The diameter of SWNTs is measured by a transmission electron microscopy (TEM) (Figure 1c, inset). Both the SEM and TEM images (Figure 1c) confirm that our as-grown SWNTs present high purity and quality, and thus do not need any purification process. This greatly simplifies the fabrication and integration process for our SWNT photonic applications. The typical SWNT and bundle lengths are around several micrometers. The nanotube density is estimated at ≈500 nanotubes per square micrometer. In our SWNT growth process, the diameter range (from 1 to 1.3 nm, as measured by TEM, absorption, and Raman spectroscopy) of the SWNTs is specially designed to tune the SWNT bandgap to match the telecommunication band at 1.55 μm (red solid line in Figure 1d) for resonant nonlinearity enhancement. A strong absorption peak (Figure 1d) occurs at ≈1550 nm, corresponding to the first transition in semiconducting SWNTs.[27] The spectral features at ≈900 nm and shorter wavelengths are the second and higher transitions.[27] The deduced diameter distribution from the transmittance spectrum is ranging from 1.0 to 1.3 nm.[27] The optical transmittance of the SWNT thin film is about 57% at the wavelength of 1550 nm, with a thickness of ≈100 nm.[28]

Figure 1e depicts Raman spectrum of the SWNT film sample using an excitation photon energy of 1.96 eV (633 nm). As expected, the Raman spectrum exhibits a very strong graphite mode (known as G band) and radial breathing modes (RBMs), which are characteristic features of SWNTs. The G band is related to the vibration of sp^2-bonded carbon atoms in a 2D hexagonal lattice of the graphite layer,[29] while the defect band (known as D band) located at ≈1337 cm^{-1} corresponds to

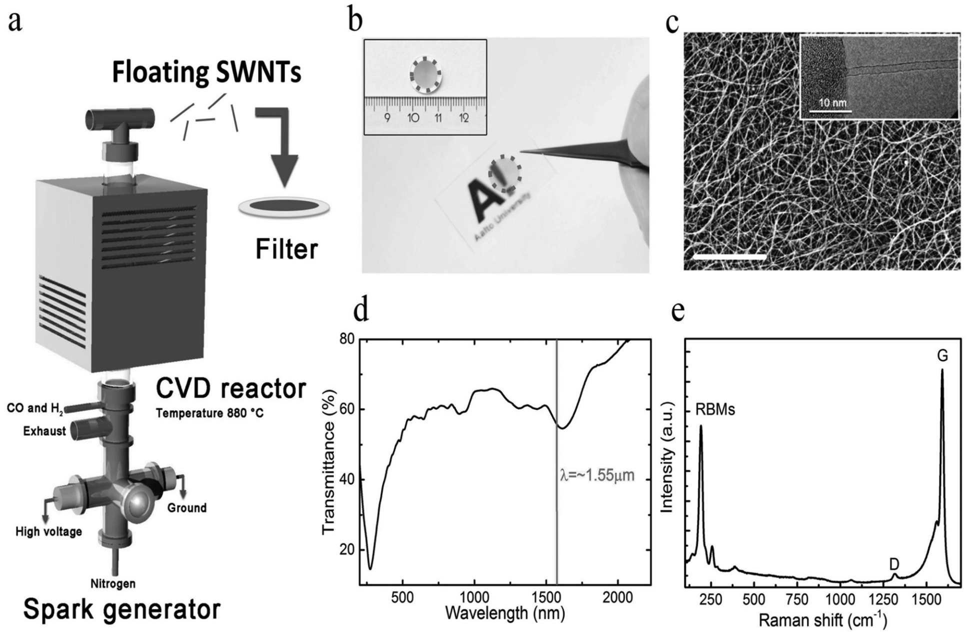

Figure 1. SWNT device fabrication and characterization. a) SWNT growth setup. b) The SWNT device was directly fabricated by dry transferring of a SWNT network film (inset, collected by direct filtration from the reactor) on a fused quartz substrate. The red dotted circles indicate the SWNT thin film. c) High-resolution image of the SWNT device with scanning electron microscope (inset, transmission electron microscopy image of a low density SWNT device for nanotube diameter measurement). The scale bar: 600 nm. d) Transmittance spectrum and e) Raman spectrum of the SWNT device.

the presence of defects on the nanotube walls or amorphous carbon materials in the sample.[29] Therefore, the intensity ratio of G and D bands (I_G/I_D) has long been used to indicate the SWNT quality.[29] The very high I_G/I_D ratio of ≈34 (as shown in Figure 1e) exhibits the good quality of our SWNTs. The very pronounced RBM peaks also imply the high quality of SWNTs, and the main peak at ≈191 cm^{-1} corresponds to the SWNT diameter of ≈1.24 nm due to the reverse relationship of RBM frequency (ω_{RBM}) and diameter (d) ($\omega_{\mathrm{RBM}} \approx \frac{214.4\ \mathrm{cm}^{-1}}{d} + 18.7\ \mathrm{cm}^{-1}$[30]). This result is in good agreement with the TEM (Figure 1c) and optical transmittance (Figure 1d) measurements, confirming the SWNT diameter distribution from 1 to 1.3 nm as designed.

Our first demonstration is to measure the conversion efficiency of stimulated FWM process in our carbon nanotube device. We use the stimulated FWM process in a pump–probe configuration as shown in **Figure 2** (details as described in the Experimental Section). The pump beam is from a mode-locked fiber laser at the wavelength of 1550.1 nm, and the probe beam is obtained from a fiber laser with peak power of 0.1 W at the idler wavelength of 1555.68 nm. With such a thin layer (≈100 nm) of SWNTs, we measure the generated signal at 1544.56 nm by using an avalanche photodiode (APD1). We plot the ratio between the signal power (P_s) and the idler power (P_i) as a function of the pump power (P_p) for the SWNT device and a reference fused quartz device in **Figure 3**. The conversion efficiency of stimulated FWM process in the SWNTs has a quadratic dependence on power, as shown in Figure 3. With this stimulated FWM process, we can estimate various nonlinearities (nonlinear refractive index n_2, parametric nonlinearity γ, and Raman gain g) in our SWNTs. In the SWNT results, we have subtracted the counts that are generated in the fused quartz substrate (inset of Figure 3). Note that the thickness of the SWNT nanofilm is 10^4 times thinner than the reference quartz sample (≈1 mm), but the conversion efficiency of the SWNT film is about ≈100–1000 times larger than the reference quartz sample. It has been pointed out that supporting substrates of nanotubes can cause depolarization of light and the broadening of the excitonic transitions.[31] However, we did not observe any significant change of signal counts at the interface between the SWNT film and the fused quartz substrate by adjusting the delay of the device with respect to the pump and the idler. This denotes that nonlinear optical interaction at the interface between the SWNTs and the quartz substrate does not contribute to the photon-pair generation.

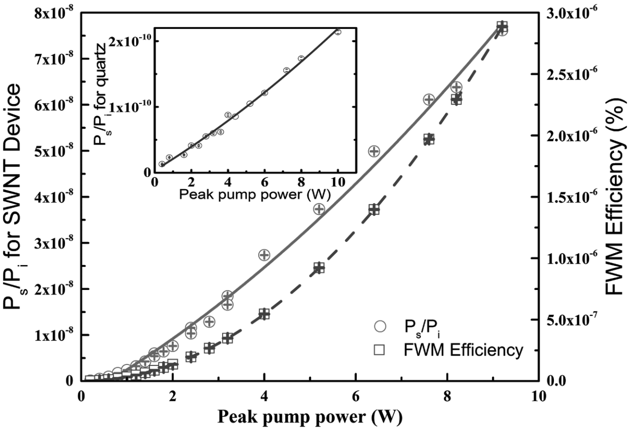

Figure 3. The ratio of P_s/P_i and the conversion efficiency for the SWNT device in the stimulated FWM process. The solid line is the fitting curve. The dashed line is the fitting curve for the quadratic component only. Inset is the ratio of P_s/P_i for the reference fused quartz device. Error bars for each data point are included.

We fit the plots of the SWNTs and the fused quartz (Figure 3) with a quadratic polynomial function of pump

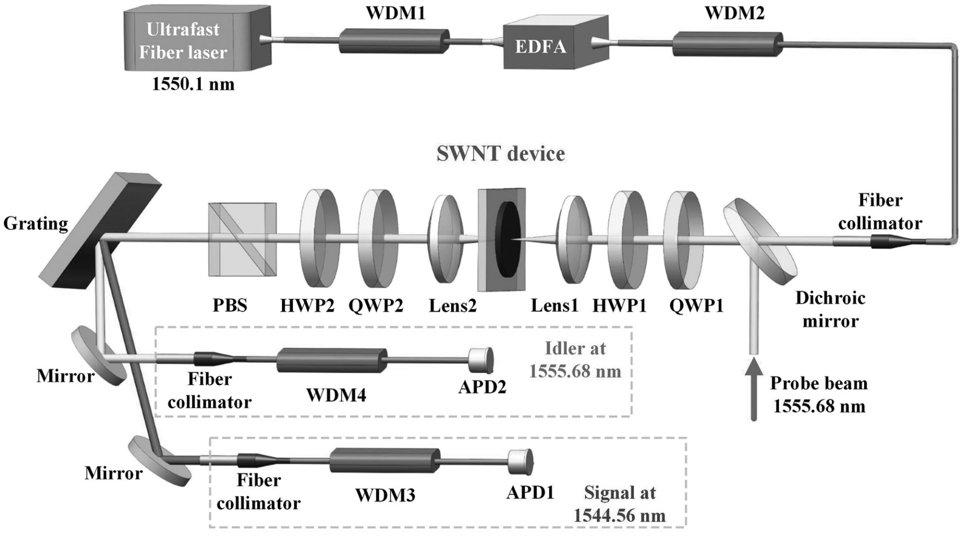

Figure 2. The experimental setup for generating and characterizing photon pairs in SWNTs. A stimulated FWM experiment is also shown, where a dichroic mirror is inserted after the fiber collimator to couple an idler probe beam at 1555.68 nm. The dichroic mirror is removed when we perform photon-pair generation experiment (i.e., no input beam at 1555.68 nm). In this case, two pump photons scatter through the Kerr-nonlinearity in SWNTs and create an energy-time entangled signal-idler photon pair at the wavelengths of 1544.56 and 1555.68 nm. WDM1, WDM2, WDM3, and WDM4: wavelength-division multiplexing filter; EDFA: Erbium-doped-fiber-amplifier; QWP1 and QWP2: quarter-wave plate; HWP1 and HWP2: half-wave plate; PBS: polarizer beam splitter. APD1 and APD2: avalanche photodiode.

power (P_p), $m_0 + m_1 P_p + m_2 P_p^2$. The parameters of m_1 and m_2 typically relate to Raman gain and nonlinear refractive index of the sample.[9] Since the SWNT device and the reference fused quartz device share the same geometry factors and detection efficiency, we obtain $\frac{m_2^{\mathrm{SWNT}}}{m_2^{\mathrm{q}}} = 762$, which is given by $\frac{0.57\,\gamma_{\mathrm{SWNT}}^2\,L_{\mathrm{SWNT}}^2}{\gamma_{\mathrm{q}}^2\,L_{\mathrm{q}}^2}$, where $\gamma = \frac{2\pi n_2}{\lambda A_{\mathrm{eff}}}$ is nonlinear parameter, and the factor of 0.57 is the transmittance of the SWNTs at ≈1.55 µm. n_2 is nonlinear refractive index, λ is the optical wavelength, and A_{eff} is the effective area. The labels of SWNT and q in the superscript/subscript of parameters indicate properties of the SWNT film and the reference quartz sample, respectively. For example, L_{SWNT} and L_{q} are the thickness of the SWNT thin film and the reference quartz substrate. Then, we obtain the nonlinear refractive index for the SWNTs as $n_2^{\mathrm{SWNT}} \approx (1.27 \pm 0.21) \times 10^{-14}\,\mathrm{m^2 W^{-1}}((2.2 \pm 0.4) \times 10^{-8}\ \mathrm{esu})$ with the help of the known nonlinear refractive index n_2^{q} for the fused quartz $\approx 3.5 \times 10^{-20}\,\mathrm{m^2\,W^{-1}}$.[32] Our estimated value of n_2^{SWNT} is around five orders of magnitude higher than the reference fused quartz (n_2^{q}). The value of n_2^{SWNT} is around one to two orders of magnitude higher than those typically reported in the literature for SWNTs.[33,34] This can be attributed to the fact that our SWNTs are specifically grown for introducing resonant nonlinearity enhancement at our experimental wavelength of ≈1.55 µm.[35] With the effective area of ≈80 µm^2, we obtain the nonlinear parameter $\gamma_{\mathrm{SWNT}} \approx (6.4 \pm 1.1) \times 10^5\ \mathrm{W^{-1}\,km^{-1}}$, which is about 3×10^5 times larger than silica fibers.[9] This indicates that SWNTs have great potential for photon-pair generation through spontaneous FWM process.

From the fit, we also obtain the ratio of Raman gain coefficient between our SWNTs (g_{SWNT}) and fused quartz (g_{q}) as $\frac{m_1^{\mathrm{SWNT}}}{m_1^{\mathrm{q}}} = \frac{0.57\,g_{\mathrm{SWNT}}\,L_{\mathrm{SWNT}}}{g_{\mathrm{q}}\,L_{\mathrm{q}}} = 332$. By using the Raman gain coefficient of silica ($g_{\mathrm{q}} = \approx 10^{-13}\ \mathrm{m\,W^{-1}}$[9]), we estimate the Raman gain coefficient of our SWNTs (g_{SWNT}) to be $\approx (5.8 \pm 0.81) \times 10^{-7}\ \mathrm{m\,W^{-1}}$, i.e., ≈10^6 times larger than the silica. Such large Raman gain coefficient in SWNTs suggests the potential coupling between Raman scattering and FWM. This also implies the potential applications of SWNTs for Raman amplification and supercontinuum generation with SWNT integrated nanoscale photonic devices.

Consequently, we remove the dichroic mirror in the pump path and perform photon-pair generation in SWNTs (Figure 2). In the spontaneous FWM process used for photon-pair generation, two pump photons at frequency ω_p scatter through the χ^3 nonlinearity in a nonlinear medium and create a correlated signal-idler photon-pair at frequencies ω_s and ω_i. Typically, in FWM-based photon-pair sources, Raman scattering inevitably occurs and generates uncorrelated photons into the signal and idler channels, leading to the degradation of quantum correlation (i.e., decreasing the CAR). For example, in our experiment, the signal and idler generated through the spontaneous FWM process are copolarized with the pump, quadratically dependent on the pump power, and spectrally correlated with the relationship of $2\,\omega_p = \omega_s + \omega_i$ due to the law of conservation of energy. However, in spontaneous Raman scattering process, a single pump photon scatters inelastically by annihilating (anti-Stokes process) or creating (Stokes process) a vibrational phonon. As a consequence, the generated Raman anti-Stokes and Stokes photons will appear in the signal and idler channels, respectively. The spontaneous Raman photons are randomly polarized in average, linearly dependent on the pump power, and spectrally uncorrelated. As we increase the pump power, the stimulated Raman scattering process occurs such that only the Stokes (idle) photons experience exponential gain. The stimulated Raman photon is copolarized with the pump, also linearly dependent on pump power and spectrally uncorrelated. As we further increase the pump power, the coupling between stimulated Raman scattering and FWM[36] normally results in the growth of anti-Stokes (signal) photons. Therefore, it is a fundamental challenge to distinguish the generated photon pairs from the noise photons. On the other hand, it is of both fundamental interest and technological importance to understand various nonlinear optical dynamics.

In general, the number of signal (N_s) and idler (N_i) photons per pulse generated through the Kerr- nonlinearity with FWM process can be written as $N_{s(i)} = S_{1,s(i)}\,N_p + S_{2,s(i)} N_p^2$,[37] where N_p is the number of pump photons per pulse, $S_{1,s(i)}$ and $S_{2,s(i)}$ are the linear and quadratic power dependence scattering coefficients for the signal (idler). Physically, $S_{1,s(i)}$ is corresponding to the strength of both spontaneous and stimulated Raman scattering processes, and $S_{2,s(i)}$ is corresponding to the strength of spontaneous FWM process. According to the equation, if $S_{1,s(i)}$ is small (i.e., the Raman photons are suppressed), $N_{s(i)}$ will exhibit clear quadratic feature. On the other hand, the quadratic feature of $N_{s(i)}$ will vanish if the Raman photons (Stokes and anti-Stokes) are dominant in the signal and idler channels. In this work, when the coupling between stimulated Raman scattering and FWM occurs, the number of the generated signal and idler photons per pulse can be expressed by $N_{s(i)}^{r} = \frac{S_{1,s(i)}^{r}}{N_p} + \frac{S_{2,s(i)}^{r}}{N_p^2}$, where $S_{1,s(i)}^{r}$ and $S_{2,s(i)}^{r}$ are inverse linear and inverse quadratic power dependence scattering coefficients. The strength of $S_{2,s(i)}^{r}$ ($S_{1,s(i)}^{r}$) coefficient implies the suppression of FWM process (stimulated Raman scattering). Therefore, in experiments, we can understand various nonlinear optical dynamics (i.e., FWM, spontaneous and stimulated Raman scattering processes) and their coupling by characterizing the photon pairs generated in our device by photon counting on signal and idler channels and performing the CAR measurement.

Hence, we first measure the generated signal and idler photons both from the SWNT device and the fused quartz reference device to fully understand various nonlinear optical dynamics. We minimize the noise photons in the photon-pair channels by using spectral and polarization filtering. The single counts of the signal and idler generated from the fused quartz as a function of the pump power are recorded (Figure S1, Supporting Information). After subtracting the counts generated in the fused quartz, we obtain the signal and idler generated from the pure SWNT nanofilm, as shown in **Figure 4**. Each data point is obtained with the integration time of 1.7 min. We can identify the generation of the signal and idler into two operation regions with respect to the peak pump power below and above 11 W. When the peak pump power is <11 W, the idler shows the linear and quadratic dependence on power (Figure 4a). This indicates that the idler is dominated by spontaneous Raman

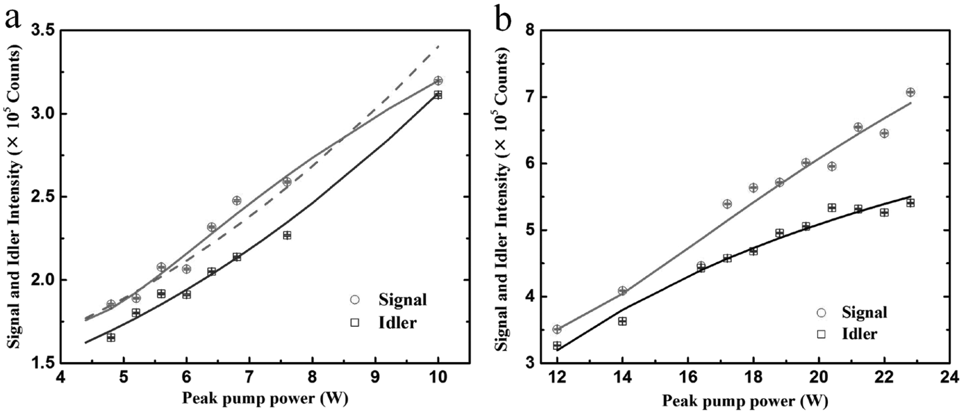

Figure 4. The signal and idler counts as a function of peak pump power per 1.7 min; a) <11 W and b) >11 W. Circle (square): the signal (idler) from the SWNTs. In (a), blue, red dashed, and green lines are the fitting results of N_i for the idler, N_s, and N_s^r (green line) for the signal, respectively. In (b), the fitting curve of N_i^r (black line) is for the idler, and N_s^r (green line) for the signal. Error bars for each data point are included.

scattering and spontaneous FWM. After fitting the idler with N_i, we find that the signal exhibits coupling between the spontaneous FWM and the stimulated Raman scattering. We then fit the signal with N_s^r (green lines in Figure 4). Since the signal and idler are generated in pairs, we plot N_s (red dashed line in Figure 4a) for the signal to compare with N_s^r. The fit shows that both signal and idler have some contributions from spontaneous FWM, but the signal is dominated by the coupling when we increase the pump power. It indicates that the stimulated Raman scattering is mediated by the spontaneous FWM, which is favored by the signal (i.e., anti-Stokes scattering process). Such observation (i.e., the growth of the anti-Stokes photons through the coupling) agrees well with the theoretical prediction,[38,39] and also has been observed in supercontinuum generation experiments.[40,41] Later, we observe the maximum CAR > 18 in this power region (i.e., <11 W) because of the unique quantum correlation of photon pairs generated by the spontaneous FWM in spite of strong stimulated Raman scattering in the signal.

When the peak pump power is >11 W, both the signal and idler exhibit coupling between spontaneous FWM and stimulated Raman scattering (Figure 4b). We fit the signal and idler with $N_{s(i)}^r$ and observe that the photon pairs are generated through an inverse quadratic function of pump power with the strength coefficient of $S_{2,s(i)}^r$. We believe that the signal and idler of the FWM process contribute as seed photons for stimulated Raman scattering, and hence suppress the quadratic power dependence of the signal and idler. Since the growth of Raman Stokes and anti-Stokes remains constant, the gain of FWM is also constant because of the suppression. This suppression scenario occurs as the signal and idler are asymptotically approaching saturation. We confirm this scenario by observing a plateau value of CAR ≈ 6 at the peak power >11 W (**Figure 5**).

Recently, there are interesting discussions on how to scale the classical and quantum devices by comparing quantum and classical nonlinear processes in traditional integrated bulk devices.[43,44] Here, let us discuss the comparison of the quantum and classical optical fields generated at the nanoscale level. The signal and idler generated through the coupling between spontaneous FWM and stimulated Raman scattering can be expressed as follows[36]

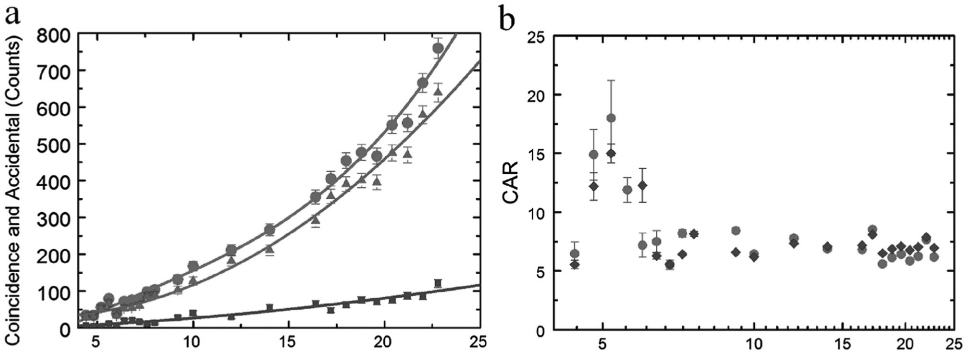

Figure 5. a) The coincidence (circle), accidental (square), and true coincidence (triangle) for the signal and idler generated in SWNTs as a function of pump power per 1.7 min. b) The CAR as a function of pump peak power. The coincidence, accidental, and CAR are reported with the subtraction of detector dark counts. Diamond: The CAR for the whole SWNT device (i.e., the SWNT film on the fused quartz substrate). Circle: The CAR for the pure SWNT nanofilm only (i.e., after subtracting the contribution from the fused quartz substrate). The raw CAR and theoretical fit[42] is given in Figure S5 (Supporting Information).

$$N_{\mathrm{s(i)}}^{\mathrm{r}} \propto \left(1-\frac{a|\beta_2|\Omega^2}{\gamma\left(a^2+b^2\right)P_{\mathrm{p}}}+\frac{\left(\beta_2\Omega^2\right)^2\left(3a^2-b^2\right)}{4\gamma^2\left(a^2+b^2\right)^2P_{\mathrm{p}}^2}\right) \tag{1}$$

where $a=1-f_{\mathrm{R}}, b=f_{\mathrm{R}}\,Re[\chi_{\mathrm{R}}^{(3)}(\Omega)]$, and f_{R} is the fractional contribution of the Raman susceptibility $\chi_{\mathrm{R}}^{(3)}(\Omega)$ to the instantaneous Kerr effect,[9,36] β_2 is the second order dispersion of carbon nanotubes, and $\Omega = |w_{\mathrm{p}} - w_{s(\mathrm{i})}|$ is the detuning of the signal and idler from the pump. $\beta_2\Omega^2$ is phase mismatch due to the dispersion of SWNTs, which can be compensated with the pump power P_{p} as $2\gamma P_{\mathrm{p}}$.[9] From Equation (1) and $N_{\mathrm{s(i)}}^{\mathrm{r}}$'s definition in the previous discussion, we obtain $|S_{1,\mathrm{s(i)}}^{\mathrm{r}}|=\frac{a|\beta_2|\Omega^2}{\gamma(a^2+b^2)}$ and $|S_{2,\mathrm{s(i)}}^{\mathrm{r}}|=\frac{(\beta_2\Omega^2)^2(3a^2-b^2)}{4\gamma^2(a^2+b^2)^2}$. The ratio of $\frac{|S_{2,\mathrm{s(i)}}^{\mathrm{r}}|}{|S_{1,\mathrm{s(i)}}^{\mathrm{r}}|}$ is given by $\frac{(\beta_2\Omega^2)(3a^2-b^2)}{4\gamma a(a^2+b^2)}$. We can study the coupling dynamics between spontaneous FWM and stimulated Raman scattering as we increase the excitation pump power. We obtain $\frac{|S_{2,\mathrm{s(i)}}^{\mathrm{r}}|}{|S_{1,\mathrm{s(i)}}^{\mathrm{r}}|}$ for the signal in the pump power region below (<) and above (>) 11 W through the fit results. Since $\left(\frac{\beta_2\Omega^2}{\gamma}\right)_< = \left(\frac{\beta_2\Omega^2}{\gamma}\right)_>$, $a_< \approx a_>$, and $a_{<\,(>)} > b_{<\,(>)}$ at the transition between the two regions, we obtain $\left(\frac{b_<}{a_<}\right)^2 \approx 1+2\times\left(\frac{b_>}{a_>}\right)^2$, indicating $\frac{b_<}{a_<}>\frac{b_>}{a_>}$ or $b_< > b_>$ at the transition. This scenario implies the reduction of f_{R} as we increase the pump power, i.e., the stimulated Raman scattering process is mediated by FWM process.

Now, we can obtain β_2 for the SWNT device with the assumption that $a_>$ is much larger than $b_>$ (i.e., $a_> \approx 1$) in the region $P_{\mathrm{p}} > 11$ W (Figure 4b). From the above fit, the ratio of $|\frac{S_{2,\mathrm{s}(i)}^{\mathrm{r}}}{S_{1,\mathrm{s}(i)}^{\mathrm{r}}}|_> \approx \frac{(\beta_2\Omega^2)^3}{4\gamma} \approx 5\,\mathrm{W}$. Then, we can estimate $|\beta_2| \approx (7.0 \pm 2.8) \times 10^6$ ps^2 km^{-1} with the help of the measured $\gamma_{\mathrm{SWNT}} \approx (6.4 \pm 1.1) \times 10^5$ W^{-1} km^{-1}. β_2 of the SWNT device is about 10^5 times larger than the fused silica (25 ps^2 km^{-1}). Note that $2\gamma P_{\mathrm{p}}$ will compensate the phase mismatch of the propagation constants of the pump, signal and idler (i.e., $|\beta_2\Omega^2| \approx |2\gamma P_{\mathrm{p}}|$), where the group velocity dispersion ($D=-\beta_2\frac{2\pi c}{\lambda^2}$) is anomalous. As for the idler, we observe that the coupling only occurs in the region above 11 W, so we cannot perform the above analysis on the idler. At the peak pump power below 11 W, the coupling in the idler is weak compared to spontaneous FWM and spontaneous Raman scattering.

After, we measure the coincidence and accidental counts as a function of pump power for the SWNT device and the fused quartz reference sample (see Figure S2 in the Supporting Information). After subtracting the contribution from the fused quartz, we obtain the coincidence, accidental and true coincidence for the thin layer of pure SWNTs as shown in Figure 5a. We then plot the CAR in Figure 5b. We observe a maximum CAR of 15 for the SWNT film on the fused quartz substrate. After the subtraction of the coincidences and accidentals from the reference fused quartz, we obtain the maximum CAR of 18 for the pure SWNT film. The maximum CAR occurs at the peak pump power ≈5.3 W, and we have coincidence counts (cc) of 54 and accidental counts of 3 within the integration time of 1.7 min. Note that the true coincidence is 54 − 3 = 51 cc, which is the contribution from photon pairs generated through spontaneous FWM process. Considering the total detection efficiency (about 0.5% for the signal, 0.6% for the idler), we have 51/(0.6% × 0.5%) = 1 700 000 cc per 1.7 min. This corresponds to ≈16 667 photon pairs per second with our carbon nanotube device. Since we use the pump laser with the repetition rate of 50 MHz, we have the photon-pair production rate of $P_{\mathrm{r}} \approx \frac{16\,667}{50\times10^6} \approx 3.3\times10^{-4}$ per pulse, comparable to these photon-pair source-based on photonic crystal fibers (see Table S1 in Supporting Information). Note that SWNTs and optical fiber-based photon-pair sources are both compatible with the existence optical fiber network for developing long distance quantum communication.

The signal and idler photons generated from spontaneous FWM process contribute to true coincidences. As we increase the pump power above 11 W, the CAR reaches the plateau value of 6 for the peak power greater than 11 W. This is due to that spontaneous FWM process is strongly coupled with stimulated Raman scattering, but the spontaneous FWM keeps the CAR ≈6. This observation can be attributed to constant $|\frac{S_2^{\mathrm{r}}}{S_1^{\mathrm{r}}}|$ in the region above 11 W, where $|\beta_2\Omega^2| \approx |2\gamma P_{\mathrm{p}}|$ and $N_{\mathrm{s(i)}}^{\mathrm{r}}$ of Equation (1) approach constant. The coupling between FWM and stimulated Raman scattering leads to the constant growth of Raman Stokes and anti-Stokes,[36] and the suppression of quadratic power dependence growth of photon-pairs through S_2^{r}. The nonlinear optical process behind the plateau feature of the CAR exhibited by the thin layer of carbon nanotubes is a surprising result and different from the fiber-based photon-pair sources, where the CAR deceased as a function of $1/P_{\mathrm{s}}$.[4,5,42] This feature indicates that the SWNTs are immune to multi-photon effects at high pump power.

A maximum CAR of ≈18 achieved here at the nanoscale dimension is comparable with other FWM-based traditional photon-pair sources at the telecom band working at room temperature (e.g., CAR ≈ 14–47 with a ≈96 μm long silicon-on-insulator waveguides,[8] ≈20 with a 25 m long photonic crystal fiber,[45] see Table S1 in Supporting Information for detailed comparison with the state of the art photon-pair generation techniques). The silicon microrings can provide CAR from 55 to 80 for the photon pairs at the telecom wavelengths by using the laser pump pulse at the repetition rate of 5 MHz.[46] Continuous-wave pumped microresonator[47] can provide photon pair production rate of 10^7 pair per second at 1 mW average pump power. However, the repetition rate of these devices is constrained by the narrow resonance spectra bandwidth. Worth noting that our nanometer scale SWNT film represents a ≈10^3 times smaller footprint than the smallest existing devices,[6–8] suitable for diverse integrated photonic applications. For example, it can provide the two-photon polarization-entangled state with the visibility of two-photon interference $\frac{\mathrm{CAR}-1}{\mathrm{CAR}+1} \approx 90\%$, which can be used for quantum simulation of integrated quantum logic gates at the nanoscale level.[48] Our SWNT-based photon-pair source also can be used as a heralded single-photon source with the estimated second-order intensity correlation function[49] $g^2(0) \approx 4/\mathrm{CAR} = 4/18 \approx 0.2$. This is better than the observed $g^2(0) = 0.32$ of the single photon source generated through the photoluminescence of individual SWNT at

298 K.[21] In-line with the development of high efficient single photon source, the CAR of 18 can be further improved by spatially multiplexing multiple such photon-pair sources.[50] The spatially multiplexing can be achieved by using the same SWNT device-based optical switch, where the working principle is based on cross-phase modulation.[51] For example, with the measured (coherent effect) nonlinear refractive index $n_2^{\mathrm{SWNT}} =\approx (1.27 \pm 0.21) \times 10^{-14}\,\mathrm{m^2 W^{-1}}$, the pump energy per pulse required for a π-phase shift is 100 nJ. Note that it is necessary to reduce the energy per switching operation for complementary metal-oxide semiconductor (CMOS)-compatible photonic integrated circuits.

Further, correlated photon pairs have been used to demonstrate quantum random walks in waveguide array,[52] heralded single photon source,[49,53] and universal linear optics protocol for linear optics quantum computing[54] (such as linear optic quantum logic and controlled NOT gate to entangle the correlated photon pairs). The quantum correlation results confirmed by measuring the CAR with 1 nm bandwidth of the idler and the signal photons indicate that our photon-pair source has excellent single spatial mode purity and therefore is suitable for quantum information processing which requires multiple quantum operations. Our source also has the compatibility advantage with current optical network systems.

Our experiments discover that the strong coupling between Raman scattering and FWM limits the photon-pair generation performance in SWNTs. This indicates that the performance of our SWNT device can be greatly improved by suppressing Raman scattering. For example, Raman spectra for SWNTs have been effectively observed at the resonance bands[29] with excitation polarization parallel to the tube axis.[55] Therefore, further experiments can be tried to reduce the contribution of Raman photons by selecting signal/idler photon pairs at small detuning from the pump, or using polarizers to remove the cross-polarized Raman photons. Worth noting that cooling has been proposed to improve the performance of other material-based traditional photon-pair generators (e.g., CAR > 100 with dispersion-shifted fiber[4] and highly nonlinear fiber[5] at 77 K). In our experiment, cooling the SWNT device can also be an effective approach to improve our SWNT device performance, as it can reduce the strength of vibrational Raman modes, and hence suppressing Raman scattering. Comparing with the traditional waveguide-based devices (e.g., photonic crystal fibers and silicon waveguides), which suffer from serious dispersion mismatch issues when cooling down for performance improvement,[46] our nanotube device will experience no dispersion mismatch problem. For example, by cooling SWNTs to 4 K,[18–20] the Bose phonon population for signal (idler) can be suppressed by a factor of 3.4×10^4. Given by a reasonably achievable phonon population reduction of >100,[18–20] we can estimate the maximum CAR of $> \frac{18}{\frac{1}{100}} = 1.8 \times 10^3$ due to the strongly suppressed stimulated Raman scattering. This will increase the visibility of two-photon interference to 99.8%, which deserves further study.

In conclusion, we demonstrate the generation of photon pairs with nanoscale nonlinear optics through spontaneous FWM process in SWNTs at the telecom wavelength. The maximum CAR of 18 with the SWNTs at room temperature was achieved. We observe that the dominant noise photons are generated from Raman scattering, which leads to the coupling between FWM and stimulated Raman scattering at relatively high peak pump power. The new observation on SWNTs will provide a new insight for exploring Raman scattering in nanoscale SWNTs for various applications (amplification and supercontinuum generation). Most importantly, our results indicate that nanoscale SWNT devices are a promising (with nonlinear refractive index five orders of magnitude larger than the currently widely used fused silica materials) nonlinear nanomaterial suitable for manipulating and generating light for quantum information processing at the nanoscale level. Our results also show that four-wave mixing process could be attributed to the collective coherence effect of individual SWNTs. Further studies on photon-pair generation in isolated SWNTs (or a free-standing SWNT film) and other low dimensional nanomaterials (e.g., graphene, other 2D layered materials and their heterostructures[56]) with high-nonlinearity can potentially lead to the demonstration of nanometer-scale sources for integrated quantum circuits and networks.

Experimental Section

SWNT Fabrication and Characterization: The SWNTs were synthesized using a spark discharge-based FC-CVD method with iron (Fe) particles as catalysts and carbon monoxide (CO) as carbon precursor (Figure 1a).[26] The Fe catalyst particles were produced via repetitive spark discharges between a pair of parallel Fe electrodes with a gap of ≈1 mm at a frequency of ≈1 kHz under inert N_2 flow. In the spark generator, each successive discharge evaporates atoms from the electrode surfaces, forming a cloud of supersaturated Fe vapor, which subsequently condenses into Fe particles. The catalyst containing N_2 flow, 200 $\mathrm{cm^3\ min^{-1}}$, from the spark discharge generator was then introduced to the CVD reactor together with CO and hydrogen (H_2) flows at rates of 250 and 50 $\mathrm{cm^3\ min^{-1}}$, respectively. The CO decomposed exclusively on the Fe catalyst particles, leading to growth of clean SWNTs. The temperature for SWNT growth was 880 °C. The as-synthesized SWNTs were then collected by direct filtration from the gas flow on a nitrocellulose membrane filter (Millipore, HAWP, 0.45 µm pore diameter) downstream the reactor. A thin (≈100 nm thick) but continuous network of SWNTs was thus formed on the filter, which was afterward dry transferred by pressing the SWNT network against a quartz substrate (Heraeus, HQS300, 1 mm thickness) with a mild pressure (<100 kPa).[27]

The morphology of the as-synthesized SWNTs was investigated by using SEM (Zeiss Supra 40) and TEM (a JEOL-2200FS double aberration-corrected TEM). The transmittance spectrum of SWNTs was recorded by a double beam Perkin-Elmer Lambda 900 spectrometer equipped with two excitation sources of a deuterium lamp and a halogen lamp, which covered the wavelength range from 175 to 3000 nm. A blank quartz substrate was used in the reference beam to exclude the effect of the substrate. Raman measurements were conducted with a JYHoriba LabRAM HR 800 Raman spectrometer using excitation at 633 nm (1.96 eV).

An ultrathin (≈100 nm thick) and uniform network of SWNT film was collected on a filter by direct filtration from the gas flow on a nitrocellulose membrane filter downstream the reactor. The as-synthesized SWNTs were afterward dry-transferred by pressing the SWNT network against a quartz substrate (Figure 1b).[27] Note that no additional purification or dispersion steps were needed prior to or during the transfer, thus rendering the SWNT film preparation rapid and compatible with various photonic and optoelectronic applications (e.g., optical fibers, silicon waveguides).[12,27]

FWM Setup: The experimental FWM setup is shown in Figure 2. A horizontally polarized pump beam at the wavelength of 1550.1 nm, pulse duration of 5 ps, and repetition rate of 50 MHz is spectrally carved out from a mode-locked ultrafast fiber laser. The pump light was amplified by using an Erbium-doped-fiber-amplifier (EDFA). The amplified spontaneous emission noise from the EDFA was suppressed by using two cascaded wavelength-division multiplexing (WDM) filters (i.e., WDM1 and WDM2) with the 3 dB bandwidth of 1 nm. The amplified pump beam was then launched to the sample via fiber-to-free space collimators. A quarter-wave plate (QWP1) and a half-wave plate (HWP1) were used for compensating the birefringence of the horizontally polarized pump beam. The pump beam was then focused into a sample by using a lens (Lens1) with a focal length of 11 mm. The beam waist of the focus spot is around ≈5 µm, with the confocal parameter ≈60 µm. The sample was a thin layer of carbon nanotubes with thickness of ≈100 nm, which was deposited on a 1 mm thick fused quartz slide. The pump beam was first propagating to the carbon nanotubes with the transmittance of 57%, and then to the quartz slide, which was experiencing 57% of the incidence pump power. The pump beam, signal, and idler at the output of the sample (carbon nanotubes and the fused quartz slide) were collimated by using a lens (Lens2) with the similar focal length of the input lens. A polarization analysis component, which consisted of a half-wave plate (HWP2), a quarter-wave plate (QWP2) and a polarizer beam splitter (PBS), was used to compensate the birefringence of the signal and idler generated in the carbon nanotubes and to reject cross-polarized Raman photons. The signal and idler were then separated from the pump beam by using a free-space grating filter. The transmission spectra of the grating filter for the signal and idler are shown in Figure S5 (Supporting Information). The signal and idler at the wavelengths of 1544.56 and 1555.68 nm, respectively, were selected so that they were about 5 nm detuning from the pump wavelength. With this detuning, the free-space grating could suppress the pump photon with the isolation greater than 45 dB. A WDM filter (i.e., WDM3 and WDM4) was inserted at each of the signal and idler channels for further suppressing the pump photon with the total isolation of >100 dB. The transmission spectra for the WDM3 and WDM4 are shown in Figure S6 (Supporting Information).

CAR Characterization: Signal and idler photons were detected by fiber-coupled In-GaAs/InP avalanche photodiodes (APD) (Model:CPS-1000, Nucrypt LLC) operated in gated Geiger mode at room temperature. The APDs were gated by 1 ns at the full-wave-half-maximum (FWHM) gate pulses at the rate of 50 MHz, which were triggered from the laser pump pulses. The timing of gate pulses for each APD could be independently adjusted by digital delay generators to coincide with the arrival of the signal and idler photons at the APDs. In the gated Geiger mode, quantum efficiency, dark counts probability, and FWHM detection window of APD1 (APD2) were about 2.7% (1.9%),[57] 7.0×10^{-5} (3.5×10^{-5}) and 280 ps (250 ps), respectively. Total detection efficiencies of signal and idler were about 0.6% and 0.5%, respectively, which included the propagation losses of optical components, the transmission loss of carbon nanotubes, and the quantum efficiencies of the APDs. A coincidence count was recorded when both APDs detected a photon at the same gated time interval. While an accidental count was recorded both APDs detected a photon at the adjacent gated time interval. The true coincidence of the photon-pairs was obtained by subtracting the accidental from the coincidence. The CAR was measured for characterizing the quality of photon-pairs generated in SWNTs. When the photon counting and CAR measurement for the signal and idler were performed, the HWP2 and QWP2 were adjusted in such a way that horizontally polarized signal and idler photons would pass through the PBS to the APD1 and APD2. Note that the PBS is filtering out the cross-polarized Raman Stokes and anti-Stokes photons scatter into the idler and signal channels. On the other hand, only the copolarized signal (anti-Stokes) and idler (Stokes) generated from the spontaneous FWM (Raman scattering) were detected by the APDs.

Supporting Information

Supporting Information is available from the Wiley Online Library or from the author.

Acknowledgements

This material was based upon research sponsored by AFRL (Agreement No. FA8750-15-1-0117), Academy of Finland (Grant Nos. 276160, 276376, 284548, 285972, 292600, 295777, and 304666), the European Union's Seventh Framework Programme (Grant Nos. 314068, 604472, and 631610), the China Scholarship Council, the Aalto Energy Efficiency program (MOPPI), the TEKES projects (CARLA, USG, and OPEC), the National Natural Science Foundation of China (Grant No. 51502031), and the Nokia Foundation. A.M. acknowledges support from the H2020 Marie-Sklodowska-Curie Individual Fellowship scheme. The authors also thank the provision of facilities and technical support by the Aalto University at Micronova Nanofabrication Centre and the TEM measurement results from Hua Jiang. The Contractor acknowledges the U.S. Government's support in the publication of this paper. The views and conclusions contained herein are those of the authors and should not be interpreted as necessarily representing the official policies or endorsements, either expressed or implied, of Air Force Research Laboratory or the U.S. Government.

Keywords

carbon nanotubes, four-wave mixing, nonlinear optics, photon pairs

Received: November 5, 2016
Revised: February 22, 2017

[1] J. L. O'Brien, A. Furusawa, J. Vučković, *Nat. Photonics* **2009**, *3*, 687.
[2] A. Politi, M. J. Cryan, J. G. Rarity, S. Yu, J. L. O'Brien, *Science* **2008**, *320*, 646.
[3] D. E. Chang, V. Vuletić, M. D. Lukin, *Nat. Photonics* **2014**, *8*, 685.
[4] K. F. Lee, J. Chen, C. Liang, X. Li, P. L. Voss, P. Kumar, *Opt. Lett.* **2006**, *31*, 1905.
[5] Y. M. Sua, J. Malowicki, M. Hirano, K. F. Lee, *Opt. Lett.* **2013**, *38*, 73.
[6] J. E. Sharping, K. F. Lee, M. A. Foster, A. C. Turner, B. S. Schmidt, M. Lipson, A. L. Gaeta, P. Kumar, *Opt. Express* **2006**, *14*, 12388.
[7] C. Xiong, M. J. Collins, M. J. Steel, T. F. Krauss, B. J. Eggleton, A. S. Clark, *IEEE J. Sel. Top. Quantum Electron.* **2015**, *21*, 6400510.
[8] J. He, A. S. Clark, M. J. Collins, J. Li, T. F. Krauss, B. J. Eggleton, C. Xiong, *Opt. Lett.* **2014**, *39*, 3575.
[9] Q. Lin, F. Yaman, G. P. Agrawal, *Phys. Rev. A.* **2007**, *75*, 023803.
[10] C. Reimer, M. Kues, L. Caspani, B. Wetzel, P. Roztocki, M. Clerici, Y. Jestin, M. Ferrera, M. Peccianti, A. Pasquazi, S. T. Chu, D. J. Moss, R. Morandotti, *Nat. Commun.* **2015**, *6*, 8236.
[11] P. Avouris, M. Freitag, V. Perebeinos, *Nat. Photonics* **2008**, *2*, 341.
[12] a) A. Martinez, Z. Sun, *Nat. Photonics* **2013**, *7*, 842; b) Z. Sun, T. Hasan, A. C. Ferrari, *Phys. E* **2012**, *44*, 1082; c) T. Hasan, Z. Sun, F. Wang, F. Bonaccorso, P. H. Tan, A. G. Rozhin, A. C. Ferrari, *Adv. Mater.* **2009**, *21*, 3874.
[13] J. Wang, Y. Chen, W. J. Blau, *J. Mater. Chem.* **2009**, *19*, 7425.
[14] V. A. Margulis, O. V. Boyarkina, E. A. Gaiduk, *Opt. Commun.* **2005**, *249*, 339.

[15] K. K. Chow, S. Yamashita, *Opt. Express* **2009**, *17*, 15608.
[16] H. Kim, T. Sheps, P. G. Collins, E. O. Potma, *Nano Lett.* **2009**, *9*, 2991.
[17] E. Gaufres, N. Izard, A. Noury, X. L. Roux, G. Rasigade, A. Beck, L. Vivien, *ACS Nano* **2012**, *6*, 3813.
[18] A. Hogele, C. Galland, M. Winger, A. Imamoglu, *Phys. Rev. Lett.* **2008**, *100*, 217401.
[19] Y. Miyauchi, M. Iwamura, S. Mouri, T. Kawazoe, M. Ohtsu, K. Matsuda, *Nat. Photonics* **2013**, *7*, 715.
[20] M. S. Hofmann, J. T. Gluckert, J. Noe, C. Bourjau, R. Dehmel, A. Hogele, *Nat. Nanotechnol.* **2013**, *8*, 502.
[21] X. Ma, N. F. Hartmann, J. K. Baldwin, S. K. Doorn, *Nat. Nanotechnol.* **2015**, *10*, 671.
[22] A. Srivastava, M. Sidler, A. V. Allain, D. S. Lembke, A. Kis, A. Imamoglu, *Nat. Nanotechnol.* **2015**, *10*, 491.
[23] Y. M. He, G. Clark, J. R. Schaibley, Y. He, M. C. Chen, Y. J. Wei, X. Ding, Q. Zhang, W. Yao, X. Xu, C. Y. Lu, J. W. Pan, *Nat. Nanotechnol.* **2015**, *10*, 497.
[24] M. Koperski, K. Nogajewski, A. Arora, V. Cherkez, P. Mallet, J. Y. Veuillen, J. Marcus, P. Kossacki, M. Potemski, *Nat. Nanotechnol.* **2015**, *10*, 503.
[25] C. Chakraborty, L. Kinnischtzke, K. M. Goodfellow, R. Beams, A. N. Vamivakas, *Nat. Nanotechnol.* **2015**, *10*, 507.
[26] K. Mustonen, P. Laiho, A. Kaskela, Z. Zhu, O. Reynaud, N. Houbenov, Y. Tian, T. Susi, H. Jiang, A. G. Nasibulin, E. I. Kauppinen, *Appl. Phys. Lett.* **2015**, *107*, 013106.
[27] H. Kataura, Y. Kumazawa, Y. Maniwaa, I. Umezub, S. Suzuku, Y. Ohtsuka, Y. Achiba, *Synth. Met.* **1999**, *103*, 2555.
[28] A. G. Nasibulin, A. Kaskela, K. Mustonen, A. S. Anisimov, V. Ruiz, S. Kivist, S. Rackauskas, M. Y. Timmermans, M. Pudas, B. Aitchison, M. Kauppinen, D. P. Brown, O. G. Okhotnikov, E. I. Kauppinen, *ACS Nano* **2011**, *5*, 3214.
[29] M. S. Dresselhaus, G. Dresselhaus, R. Saito, A. Jorio, *Phys. Rep.* **2005**, *409*, 47.
[30] H. Telg, J. Maultzsch, S. Reich, F. Hennrich, C. Thomsen, *Phys. Rev. Lett.* **2004**, *93*, 177401.
[31] J. C. Blancon, M. Paillet, H. N. Tran, X. T. Than, S. A. Guebrou, A. Ayari, A. San Miguel, N. M. Phan, A. A. Zahab, J. L. Sauvajol, N. Del Fatti, F. Vallee, *Nat. Commun.* **2013**, *4*, 2542.
[32] R. Adair, L. L. Chase, S. A. Payne, *Phys. Rev. B* **1989**, *39*, 3337.
[33] Y. C. Chen, N. R. Raravikar, L. S. Schadler, P. M. Ajayan, Y. P. Zhao, T. M. Lu, G. C. Wang, X. C. Zhang, *Appl. Phys. Lett.* **2002**, *81*, 975.
[34] S. Yamashita, *J. Lightwave Technol.* **2012**, *30*, 427.
[35] A. Maeda, S. Matsumoto, H. Kishida, T. Takenobu, Y. Iwasa, M. Shiraishi, M. Ata, H. Okamoto, *Phys. Rev. Lett.* **2005**, *94*, 047404.
[36] S. Coen, D. A. Wardle, J. D. Harvey, *Phys. Rev. Lett.* **2002**, *89*, 273901.
[37] X. Li, P. L. Voss, J. Chen, K. F. Lee, P. Kumar, *Opt. Express* **2005**, *13*, 2236.
[38] N. Bloembergen, Y. R. Shen, *Phys. Rev. Lett.* **1964**, *12*, 504.
[39] Y. R. Shen, N. Bloembergen, *Phys. Rev.* **1965**, *137*, A1787.
[40] S. Coen, A. H. L. Chau, R. Leonhardt, J. D. Harvey, J. C. Knight, W. J. Wadsworth, P. S. J. Russell, *J. Opt. Soc. Am. B* **2002**, *19*, 753.
[41] R. Claps, V. Raghunathan, D. Dimitropoulos, B. Jalali, *Opt. Express* **2003**, *11*, 2862.
[42] a) H. Takesue, K. Inoue, *Opt. Express* **2005**, *13*, 7832; b) K. I. Harada, H. Takesue, H. Fukuda, T. Tsuchizawa, T. Watanabe, K. Yamada, Y. Tokura, S. I. Itabashi, *IEEE J. Sel. Top. Quantum Electron.* **2010**, *16*, 325; (c) A. S. Clark, M. J. Collins, A. C. Judge, E. C. Mägi, C. Xiong, B. J. Eggleton, *Opt. Express* **2012**, *20*, 16807.
[43] L. G. Helt, M. Liscidini, J. E. Sipe, *J. Opt. Soc. Am. B* **2012**, *29*, 2199.
[44] M. Liscidini, J. E. Sipe, *Phys. Rev. Lett.* **2013**, *111*, 193602.
[45] W. Zhang, Q. Zhou, J. R. Cheng, Y. D. Huang, J. D. Peng, *Eur. Phys. J. D* **2010**, *59*, 309.
[46] R. Kumar, J. R. Ong, J. Recchio, K. Srinivasan, S. Mookherjea, *Opt. Lett.* **2013**, *38*, 2969.
[47] M. Fortsch, J. U. Furst, C. Wittmann, D. Strekalov, A. Aiello, M. V. Chekhova, C. Silberhorn, G. Leuchs, C. Marquardt, *Nat. Commun.* **2013**, *4*, 1818.
[48] I. M. Georgescu, S. Ashhab, F. Nori, *Rev. Mod. Phys.* **2014**, *86*, 153.
[49] L. Yang, X. Ma, X. Guo, L. Cui, X. Li, *Phys. Rev. A* **2011**, *83*, 053843.
[50] M. J. Collins, C. Xiong, I. H. Rey, T. D. Vo, J. He, S. Shahnia, C. Reardon, T. F. Krauss, M. J. Steel, A. S. Clark, B. J. Eggleton, *Nat. Commun.* **2013**, *4*, 2582.
[51] N. Matsuda, R. Shimizu, Y. Mitsumori, H. Kosaka, K. Edamatsu, *Nat. Photonics* **2009**, *3*, 95.
[52] A. Peruzzo, A. Peruzzo, J. C. F. Matthews, N. Matsuda, A. Politi, K. Poulios, X. Zhou, Y. Lahini, N. Ismail, K. Wörhoff, Y. Bromberg, Y. Silberberg, M. G. Thompson, J. L. OBrien, *Science* **2010**, *329*, 1500.
[53] E. A. Goldschmidt, M. D. Eisaman, S. V. Polyakov, A. Migdall, *Phys. Rev. A* **2008**, *78*, 013844.
[54] J. Carolan, C. Harrold, C. Sparrow, E. M. López, N. J. Russell, J. W. Silverstone, P. J. Shadbolt, N. Matsuda, M. I. M. Oguma, G. D. Marshall, M. G. Thompson, J. C. F. Matthews, T. Hashimoto, J. L. O'Brien, A. Laing, *Science* **2015**, *349*, 711.
[55] A. Hartschuh, H. N. Pedrosa, L. Novotny, T. D. Kraus, *Science* **2003**, *301*, 1354.
[56] a) F. Bonaccorso, Z. Sun, T. Hasan, A. C. Ferrari, *Nat. Photonics* **2010**, *4*, 611; b) Z. Sun, A. Martinez, F. Wang, *Nat. Photonics* **2016**, *10*, 227.
[57] K. Y. Wang, V. G. Velev, K. F. Lee, A. S. Kowligy, P. Kumar, M. A. Foster, A. C. Foster, Y. P. Huang, *Opt. Lett.* **2014**, *39*, 914.